ELSEVIER

Intermetallics 8 (2000) 1169–1174

Intermetallics

www.elsevier.com/locate/intermet

Extrusion and selected engineering properties of Mo–Si–B intermetallics

E. Summers, A.J. Thom *, B. Cook, M. Akinc

Ames Laboratory and Department of Materials Science & Engineering, Iowa State University, Ames, IA 50011, USA

Received 1 September 1999; accepted 31 May 2000

Abstract

In this study, an extrusion process has been developed to produce defect free, high-density rods of Mo–Si–B material. An initial powder composition (53.5 vol.%, 91 wt.%) of 66 vol.% $Mo_5Si_3B_x$ (T1)–16 vol.% MoB–18 vol.% $MoSi_2$ was mixed with a paraffin-wax based binder (46.5 vol.%, 9 wt.%) and extruded using a twin-screw extruder. Following binder removal by a combination process of wicking and thermal degradation, the material was sintered at 1800°C. The bulk density of the sintered material was 90–92% of theoretical. Thorough binder removal was evidenced by low impurity levels: 258±6 ppm carbon and 772±10 ppm oxygen. The material demonstrated excellent high temperature oxidation resistance. The calculated parabolic rate constant is 1.1×10^{-2} mg^2/cm^4/h at 1600°C. The extruded material was also successfully tested as a resistance heating element. These materials show promise for the development of heating elements with enhanced performance compared to current $MoSi_2$-based heating elements. © 2000 Published by Elsevier Science Ltd.

Keywords: A. Intermetallics, miscellaneous; A. Molybdenum silicides; Extrusion

1. Introduction

High temperature processes are becoming more and more prevalent in today's industrial society. With these processes comes the demand for improved materials that will extend the maximum operating temperature of components such as gas turbines, heat exchangers, and heating elements. Intermetallic compounds based on aluminum, silicon, and chromium have been extensively investigated for possible use at these elevated temperatures. As a practical example, $MoSi_2$ is commonly used as the resistance heating component for high temperature furnace heating elements [1]. Due to the outstanding oxidation resistance of $MoSi_2$, these elements routinely operate up to 1700°C in an air atmosphere. Recent alloy developments by heating element manufacturers have extended the operating temperature of these elements up to 1800°C. However, $MoSi_2$-based alloys exhibit poor low temperature mechanical strength and low creep resistance at high temperatures [2,3]. $MoSi_2$ is also prone to pesting [4] (catastrophic oxidation) at temperatures below 800°C. These cumulative limitations are the topic of investigation by various researchers and preclude the near term implementation of $MoSi_2$-based alloys for many high temperature applications.

Another silicide, Mo_5Si_3, is actively being investigated as a possible material for high temperature applications. While this material has superior creep resistance compared to $MoSi_2$ [5], the oxidation resistance is poor [6,7]. Research at Ames Laboratory has focused on the mechanical and physical properties of phase assemblages within the Mo–Si–B ternary phase diagram [8,9]. Two of these phase assemblages include the $Mo_5Si_3B_x$(T1)-Mo_3Si–Mo_5SiB_2(T2) ternary triangle and the T1–$MoSi_2$–MoB ternary triangle. These in-situ composites offer an interesting alternative to $MoSi_2$-based alloys. They possess oxidation resistance comparable to $MoSi_2$ [10,11] and superior creep resistance [5]. Evaluation of the mechanical properties of these two distinct phase assemblages is in preliminary stages. However, initial results suggest both improved strength and fracture toughness compared to $MoSi_2$ [12].

The objective of the present work is to demonstrate the use of these Mo–Si–B in-situ composites as a resistance heating element material. This necessitates the

* Corresponding author.

0966-9795/00/$ - see front matter © 2000 Published by Elsevier Science Ltd.
PII: S0966-9795(00)00080-7

fabrication of cylindrical rod shapes, and extrusion is a well-suited processing technique to produce rod shapes. In particular, the development of an extrusion process to produce defect-free rods consisting of the T1–$MoSi_2$–MoB phase assemblage will be discussed. Selected engineering properties, demonstrating that these rod shapes can function as a heating element material, will be presented.

2. Experimental procedure

2.1. Alloy preparation

The powder used in this investigation was obtained from commercial vendors. An Mo–Si–B powder consisting of about 80 vol.% T1 phase and 20 vol.% MoB was mixed with an appropriate amount of $MoSi_2$ powder to achieve the desired T1-MoB-$MoSi_2$ phase assemblage. The powder mix was milled and sieved through a 500 mesh screen (<25 μm) for subsequent compounding with the binder. The powder and a paraffin wax-based binder were then compounded for extrusion. The resulting feedstock consisted of 9 wt.% binder and 91 wt.% powder (46.5 vol.% binder and 53.5 vol.% powder) and was extruded using a twin-screw laboratory extruder. The feedstock was extruded through a cylindrical die (3.8 or 6.4 mm diameter) and collected on a plastic plate. Binder removal temperatures were estimated from thermogravimetric analysis experiments using small pieces of extrudate and binder. Two different techniques were used to remove binder: thermal degradation and wicking. For thermal debinding the samples were placed on Ta foil, with additional Ti sponge as an oxygen getter, and heated in a tube furnace under flowing nitrogen. During wicking the extrudates were immersed in a bed of Al_2O_3 powder and heated in a tube furnace under flowing nitrogen. After completion of the initial binder removal, the material was then sintered in a graphite element furnace under flowing argon gas. The samples were packed in coarse T1–MoB powder to provide a barrier between the sample and the graphite environment. The extrudates were heated to 1000°C for removal of the final binder component, then heated to 1800°C for sintering. Phase assemblage of the sintered material was quantified by analyzing the powder X-ray diffraction pattern using a whole-pattern refinement program. Density of the sintered extrudate was measured using the Archimedes liquid immersion technique. Carbon impurities were measured by the combustion method and oxygen impurities were measured by inert gas fusion.

2.2. Oxidation testing and heating element demonstration

For isothermal oxidation testing, coupons were suspended from a sapphire wire in a vertical tube thermogravimetric analyzer. A small hole was spark machined through the coupons from which the coupons were suspended. The samples were heated at 20°C/min in flowing compressed breathing air to the test temperature. Specimen mass change and temperature were continuously recorded. Electrical tests were performed by coating the ends of an 8.5 cm long by 0.34 cm diameter sintered rod with a conductive silver epoxy. The epoxy was subsequently cured at 600°C in an argon environment and electrical connections were accomplished by clamping 50A braided aluminum straps to the coated portions of the element using steel spring clips. A power supply (200 A, 12 VAC) was connected to the straps and the element was mounted in a specially designed firebrick and zirconia test fixture. Temperature of the element was determined by use of an optical pyrometer with corrections for emissivity of the material. Calibration of the IV characteristics of the fixture was accomplished by observing the behavior of a commercially available $MoSi_2$-based element.

3. Results and discussion

3.1. Powder characteristics

SEM analysis of the as-received T1–MoB powder revealed significant agglomeration of sub-micron sized particles. The heavy agglomeration caused a dramatic decrease in the volume loading of powder for an extrudable feedstock. For the agglomerated powder, the maximum volume loading was about 40 vol.%. This powder volume loading is very low compared to other typical feedstocks [13] that range from 50 to 70 vol.%. It is possible that the increased surface area associated with the sub-micron particles contributed to an increased binder loading.

The as-received powder was then milled to reduce particle size, and 1 wt.% stearic acid was added to the powder before milling as a grinding aid. The milled powders showed some cold welding of the smaller sub-micron particles. However, milling reduced the overall particle size, and the powder volume loading was increased to a more acceptable level of 53.5 vol.%.

3.2. Binder selection

Several organic systems were investigated as possible binders for the Mo–Si–B powder. Methylcellulose ethers were initially used, but when mixed with the powder, yielded low green strengths. Also, a significant amount of binder residue remained after removal at 500°C. This high residue content is consistent with other work in which 10.5 wt.% of the methylcellulose remains as residue after thermolysis at 1000°C in argon [13]. Consequently, methylcellulose was considered an unacceptable binder.

Acrylics were also investigated, and they gave much higher green strengths than the methylcellulose binder. Acrylics burn out cleanly in an inert atmosphere, so high residue is not expected. However, the acrylics used produced large amounts of water, approximately 70 wt.%. Water apparently reacted with the powder during thermolysis as the powder surface color changed from gray to purple, and XRD analysis showed that $MoO_x \cdot xH_2O$ had formed. Acrylics were also judged as an unacceptable binder.

A paraffin wax-based binder was then evaluated. The paraffin wax is the filler phase of the binder that principally aids in extrusion. Other higher molecular weight polymers act as a backbone providing strength once the paraffin wax has been removed. This binder gave good green strength and pyrolyzed cleanly in an inert atmosphere. Also, no water is present in the formulation so that reaction with the powder was not a concern. This binder system was used for all subsequent extrusion experiments.

The viscosity of the binder at the extrusion temperature must be considered. The binder viscosity was measured at a constant shear rate of 232 s^{-1} over the temperature range of 90–99°C, imitating the extruding and mixing temperature process. The viscosity of the binder ranged from 1.25 to 0.85 Pa•s, and this is well below the recommended value [13] of 10 Pa•s. Since the shear rate for twin-screw extruders is considerably higher than 232 s^{-1}, there was little concern of excessive binder viscosity.

3.3. Compounding and extrusion of feedstock

The actual solids loading for the powder used in this study was 53.5 vol.%. The critical solids volume loading for our feedstock and extruder combination was estimated to be approximately 57 vol.%, estimated from initial extrusion runs using solids loading exceeding 57 vol.%. These initial runs failed due to shear pin breakage in the extruder caused by excessive feedstock viscosity. The viscosity of a feedstock can be estimated from Eq. (1), which relates feedstock viscosity to the volume loading of the powder and the viscosity of the binder at the mixing temperature [13]:

$$\eta_M = \frac{(A \bullet \eta_b)}{(1 - \frac{\phi}{\phi_c})^2} \quad (1)$$

where

η_M = feedstock viscosity
A = constant dependent on the particle size and shape (typically 1)
η_b = binder viscosity (0.876 Pa•s at 95°C)
ϕ = solids volume loading (0.535)
ϕ_c = estimated critical solids volume loading (0.57)

As $\phi \rightarrow \phi_c$, the viscosity rapidly increases so that the feedstock cannot be extruded. For the actual solids loading of 0.535, the predicted feedstock viscosity is about 230 Pa•s, and this compares favorably to typical feedstock viscosities observed in powder metallurgy processing [13].

As shown in Fig. 1, the plasticity of the extrudate from the 3.8 mm die is evident as it exits the die and is easily bent at a 90° angle without causing cracking. The binder hardens within a few minutes, but the extrudate retains sufficient green strength to be easily handled without breakage or damage.

3.4. Debinding of extrudates

Critical debinding temperatures were determined from TGA analysis of the binder material. The TGA plot in Fig. 2 shows two distinct weight loss events. The initial

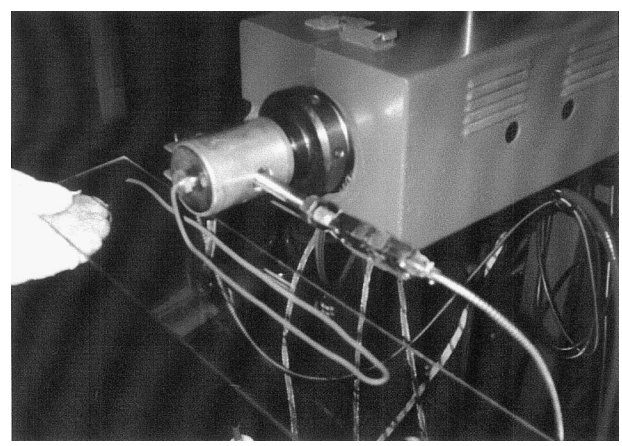

Fig. 1. Photohgraph showing the extrusion of the Mo–Si–B material. The extrudate is manually collected on a plastic plate. Note the plasticity of the material exiting the die (3.8 mm diameter) as it is immediately bent perpendicularly to the direction of extrusion.

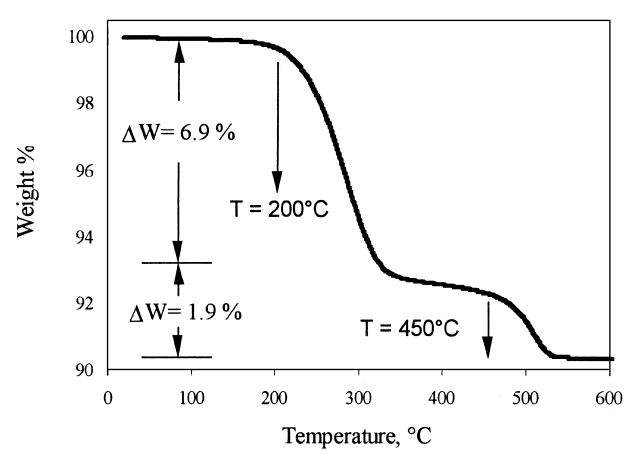

Fig. 2. TGA analysis of the feedstock (powder + binder) showing critical burnout temperatures at approximately 200 and 450°C. The test was performed under flowing nitrogen gas, heating at 10°C/min.

loss at about 200°C of 6.9 wt.% is the decomposition of the paraffin wax. The second loss at about 450°C of 1.9 wt.% is the decomposition of the higher molecular weight component. The TGA analysis predicts a total binder residue in the extrudate of about 0.2 wt.% at 600°C.

Initial debinding work utilized the thermal degradation technique, and these debinding experiments were performed prior to the TGA analysis of the binder. Initial heating rates up to 5°C/min were used in the temperature ranges of 25–200°C, and this resulted in severe defect formation. A successful thermal debinding procedure was empirically devised. The average weight loss was about 6 wt.%, indicating a residual paraffin wax content of nearly 1 wt.% when compared to the TGA analysis. This cycle was not optimized based on the TGA data, and defects were occasionally observed in the extrudates.

Because the thermal debinding process required nearly three days to remove the initial binder component, wicking was also used. Capillary forces 'wick' the binder into the alumina powder, due to a significant capillary pressure difference between the extrudate powder (20–25 μm) and the Al_2O_3 powder (0.05 μm). The wicking process was successfully used to debind samples without defect formation. Also, the time required to complete this initial debinding step was reduced to about 12 h. Using this procedure, the average weight loss of several extrudates was 6.9 wt.% ±0.5, which corresponds very closely to the initial mass loss predicted from the TGA analysis. Some wicking material adheres to the extrudate, and this contributes to the uncertainty of the mass loss measurements. The effect of this residual Al_2O_3 powder on sintering behavior and other engineering properties has not been quantified. Debinding by wicking was used for all subsequent extrusion experiments.

3.5. Sintering

Figure 3 is an optical micrograph of a sintered extrudate and demonstrates the multiphase assemblage. The relative amounts of each phase were determined by XRD/GSAS analysis of four extrudates. The range of the four samples were: 66–76 vol.% T1, 6.7–10 vol.% MoB, and 17–24 vol.% $MoSi_2$. The initial powder composition for extrusion was batched as 66 vol.% T1, 16 vol.% MoB, and 18 vol.% $MoSi_2$. There is an apparent lower MoB content in the sintered extrudate. It is possible that powder segregation occurred during compounding, contributing to an inhomogeneous phase distribution in the sintered material. It is also possible that final binder decomposition products reacted with the Mo–Si–B powder during sintering to scavenge boron. Formation of the hexagonal form of the T1 phase was seen in a fifth extrudate. Small carbon additions to tetragonal T1 phase ($Mo_5Si_3B_x$) have been shown to promote formation of the hexagonal phase [9]. The engineering properties of the hexagonal form of T1 are not known.

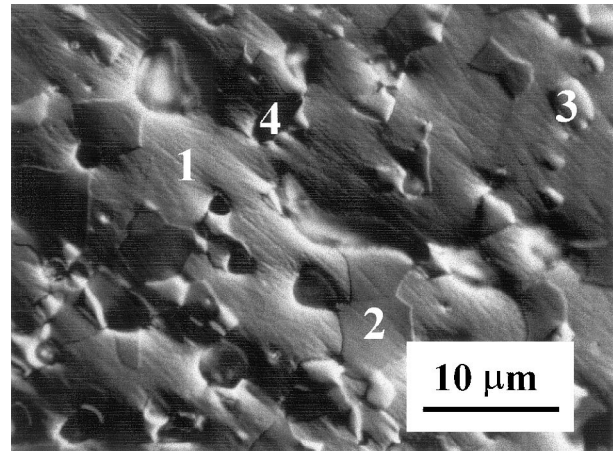

Fig. 3. Optical micrograph (Normanski Interference Contrast) of the sintered extrudate with an Archimedes density of 92% theoretical. Key: 1, T1 matrix; 2, $MoSi_2$; MoB; 4, glass/pore.

Carbon and oxygen analysis was performed on 19 sintered extrudates to quantify the extent of residual binder. While the initially extruded material contains about 9 wt.% binder, the chemical analysis of the sintered samples revealed 258±6 ppm carbon and 772±10 ppm oxygen. These data show that the wicking process for debinding and subsequent sintering cycle was extremely effective in eliminating the binder material.

The liquid immersion bulk density for the sintered extrudate was approximately 90–92% of theoretical. To establish the expected baseline density and phase assemblage of the extruded material, the Mo–Si–B powder mix was milled to <20 μm, compacted into a pellet and sintered in an argon atmosphere at 1800°C for 2 h. The phase assemblage based on XRD/GSAS analysis was 66 vol.% T1, 16 vol.% MoB, and 18 vol.% $MoSi_2$, identical to the originally batched powder mixture. The density of this sintered material was 94% of theoretical. Thus it should be possible to achieve a higher sintered density in the extruded material. However, use of a finer particle size may not work with the currently developed extrusion process, and smaller size fraction powder has not been used.

3.6. Oxidation testing

Fig. 4 shows the isothermal mass change of the sintered extrudate at 1600°C in flowing compressed breathing air. The material shows the characteristic mass gain and loss during initial heating, and this oxidation behavior for Mo–Si–B materials has been previously discussed [14]. The high temperature oxidative stability of the material is evidenced by the minimal steady state mass gain, and the oxidation process is well described by a parabolic

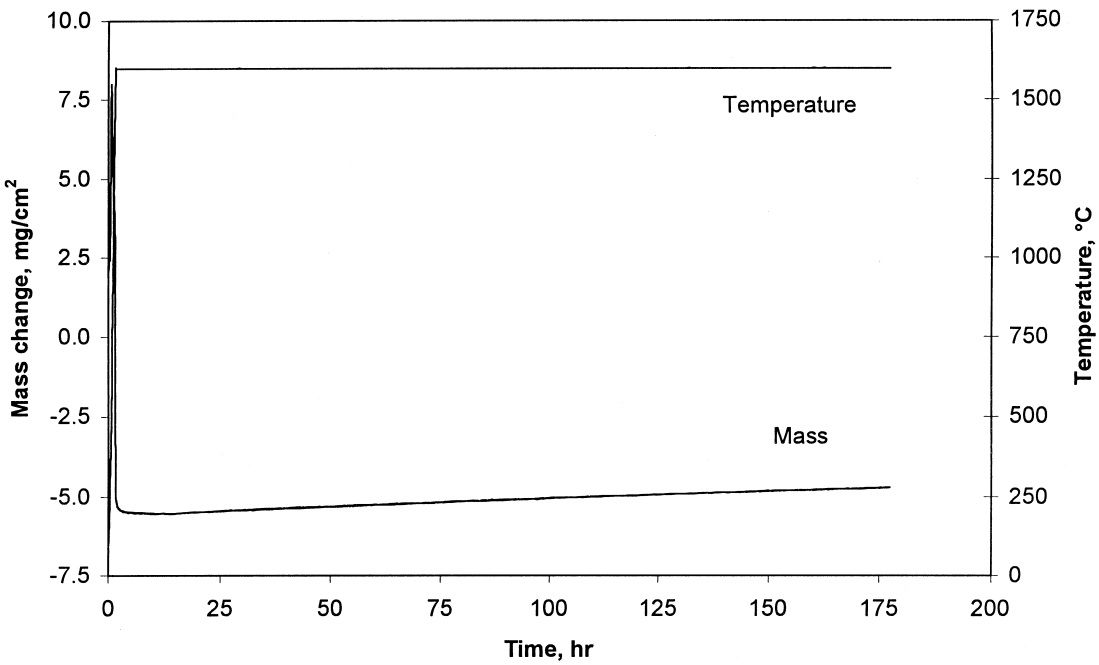

Fig. 4. Mass change of sintered extrudate during oxidation at 1600°C in flowing compressed air.

model. The calculated parabolic rate constant is 1.1×10^{-2} mg^2/cm^4/h. These rate kinetics are reasonable compared to that previously seen for T1–$MoSi_2$–MoB materials over the temperature range of 800–1450°C [10,11].

3.7. Heating element demonstration

During initial evaluation of the furnace fixture, a $MoSi_2$ element was connected and heated to 1500°C at a rate of 62°C/min. Continual adjustment of the current source was required during heat up due to the comparatively large temperature coefficient of resistivity (TCR) of the disilicide material. The power loading of the element, L, defined by

$$L = \frac{P}{A} = \frac{IV}{A}$$

where $P = IV$ is the input power to the element and A is the cross-sectional area of the active heating portion, was determined to equal 39 W/cm^2 at the maximum temperature. The resistivity was determined from the measured resistance and the ratio of cross sectional area to length of the active member. Contact resistance at the interfaces was assumed to be negligible due to the relatively high current loading. The electrical resistivity was determined to equal 0.29 mohm-cm at 1500°C, in excellent agreement with previously measured values for $MoSi_2$ using a four-point method. The Mo_5Si_3-based element was heated at the same rate as the disilicide, during which time smoke was observed indicating release of residual binder material. Formation of what is believed to be MoO_3 crystals on the surface of the element was observed to occur within the 700–1000°C temperature range. Only minimal adjustment of the current at each setpoint was required compared with the disilicide, due to the lower TCR of the Mo_5Si_3-based material. The electrical resistivity was estimated at 0.41 mohm-cm at 1000°C, which is a factor of 2–3 higher than that measured for the corresponding pressed and sintered composition using the four-point technique. The test was terminated when the center portion of the element reached 1300°C, due to the possibility of oxidation of the metal contacts and loss of continuity as a result of the large thermal gradient present in the short segment. The element was held at temperature for 10 min and allowed to furnace cool to ambient. This test was repeated 12 times and the material exhibited no indication of cracking or macroscopic creep. The power loading for this element was considerably higher than that for the disilicide element. The front wall of the furnace fixture was removed to enable visual observation of the entire element. It is remarkable that the material withstood a loading of 194 W/cm^2 at maximum temperature during these tests, far in excess of that recommended for conventional elements. Additional tests are planned with a redesigned furnace enclosure in which heat losses are minimized, allowing for a meaningful comparison of specific power dissipation characteristics with conventional $MoSi_2$. Sintering of longer rod-shaped elements is also expected to enable observation of their behavior within the targeted 1700–2000°C temperature range.

4. Conclusions

This study has demonstrated that Mo–Si–B compositions can be extruded to form high density, defect-free rods with minimal impurity levels. Densities better than 90% of theoretical were attained by sintering the extruded material at 1800°C. The extrusion process has been sufficiently refined to eliminate nearly all of the binder material. Combined carbon and oxygen impurity levels are about 1000 ppm. Material prepared by extrusion had a nominal composition of 66–76 vol.% T1, 6.7–10 vol.% MoB, and 17–24 vol.% $MoSi_2$. Extruded material demonstrates excellent oxidation resistance, exhibiting minimal parabolic mass gain at 1600°C in flowing air. The resistance heating capability of the material has also been demonstrated, functioning as a heating element in ambient air. These materials show promise for the development of heating elements with enhanced performance compared to current $MoSi_2$ based heating elements.

Acknowledgements

Ames Laboratory is operated for the US Department of Energy by Iowa State University under contract number W-7405-ENG-82. This research was supported by the Office of Basic Energy Science, Materials Science Division. This research was also supported by the Office of Energy Research, Office of Computational and Technology Research, and the Advanced Energy Projects Division.

References

[1] Bizzarri V. Electrical resistance element. US patent, 4,021,770, 3 May 1975.
[2] Sadananda K, Feng CR. A review of creep of silicides and composites. In: Briant CL, Petrovic JJ, Bewlay BP, Vasudevan AK, Lipsitt HA, editors. High temperature silicides and refractory alloys. Mat. Res. Soc. Proc., Vol. 322. Pittsburgh (PA): Materials Research Society, 1994. p. 157.
[3] Petrovic JJ. $MoSi_2$-based high-temperature structural silicides. MRS Bull 1993;18(7):35.
[4] Fitzer E. $MoSi_2$ as high-temperature material. In: Warmfeste und korrosionbestandige werkstoffe, 2. Plansee-Seminar, Springer-Verlag Wien, 1956. p. 56–79.
[5] Meyer M, Kramer M, Akinc M. Compressive creep behavior of Mo_5Si_3 with the addition of boron. J Intermetallics 1996;4:273–81.
[6] Berkowitz-Mattuck JB, Dils RR. High-temperature oxidation; II. Molybdenum silicides. J Electrochem Soc 1965;112(6):583–9.
[7] Anton DL, Shah DM. High temperature properties of refractory intermetallics. Mater Res Soc Symp Proc 1991;213:733–9.
[8] Nowotny H, Kimakopoulou E, Kudielka H. Untersuchungen in den Dreistoffsystemen: Molybdan-Silizium-Bor, Wolfram-Silizium-Bor und in dem System: VSi_2-$TaSi_2$. Mh Chem 1957;88:180.
[9] Huebsch JJ, Kramer MJ, Zhao HL, Akinc M. Solubility of boron in $Mo_{5+y}Si_{3-y}$. J Intermetallics 2000;8:143–50.
[10] Meyer MK, Akinc M. Oxidation behavior of boron-modified Mo_5Si_3 at 800–1300°C. J Am Ceram Soc 1996;79(4):938–44.
[11] Meyer MK, Akinc M. Isothermal oxidation behavior of Mo–Si–B intermetallics at 1450°C. J Am Ceram Soc 1996;79(10):2763–6.
[12] Unpublished research.
[13] German R, Bose A. Injection molding of metals and ceramics. Metal Powder Industries Federation, 1997.
[14] Meyer MK, Thom AJ, Akinc M. Oxide scale formation and isothermal oxidation behavior of Mo–Si–B intermetallics at 600–1000°C. J Intermetallics 1999;7(2):153–62.